Journal of Hazardous Materials, 7 (1982) 19—35
Elsevier Scientific Publishing Company, Amsterdam — Printed in The Netherlands

SPREADING—BOILING MODEL FOR INSTANTANEOUS SPILLS OF LIQUEFIED PETROLEUM GAS (LPG) ON WATER

H.-R. CHANG and R.C. REID

Department of Chemical Engineering, Massachusetts Institute of Technology, Cambridge, MA 02139 (U.S.A.)

(Received September 14, 1981; accepted November 13, 1981)

Summary

An experimental and theoretical investigation was carried out to study the boiling and spreading of liquefied petroleum gas (LPG) on water, in a one-dimensional configuration.

Experimental work involved the design and construction of a spill/spread/boil apparatus which permitted the measurement of spreading and local boil-off rates. With the equations of continuity and momentum transfer, a mathematical model was developed to describe the boiling—spreading phenomena of cryogens spilled on water. The model accounts for a decrease in the density of the cryogenic liquid due to bubble formation.

The boiling and spreading rates of LPG were found to be the same as those of pure propane. An LPG spill was characterized by the very rapid and violent initial boiling and highly irregular ice formation on the water surface. The measured local boil-off rates of LPG agreed well with theoretical predictions from a moving-boundary heat-transfer model. The spreading velocity of an LPG spill was found to be slightly less than predicted by the spreading model as the rough ice formed on the surface impeded the flow of the LPG.

Notation

A	cross-sectional area for vapor flow (m^2)
C	gas concentration (kg m^{-3}); C_T, tracer; C_H, hydrocarbon
F	force (Pa); F_{gr}, gravitational; F_{in}, inertial
g	acceleration due to gravity (m s^{-2}); $g^\star$, effective g defined by eqn. (5)
h	height of cryogen film (m)
$h^\star_{nb}$	$h/(V_L x_{e_{nb}} w)$
$h^\star$	$h/(V_o/x_e w)$
ΔH_V	enthalpy of vaporization (kJ kg^{-1})
k	parameter in eqn. (10)
$\dot{M}$	boiling flux (kg m^{-2} s^{-1})
$\dot{Q}$	boiling heat transfer flux (kJ m^{-2} s^{-1})
t	time (s); t_o, defined by eqn. (15)
$t_{e_{nb}}$	$x^3_{e_{nb}}$ $(g^\star V_L/w)^{1/2}$; (s)
t_e	characteristic time (s); $[(V_o/w)^2/(\dot{M}/\rho)^3 g^\star]^{1/5}$
$t^\star_{nb}$	$t/t_{e_{nb}}$

0304-3894/82/0000—0000/$02.75

$t^{\star}$ t/t_e
u gas velocity (m s^{-1})
u_B bubble rise velocity (m s^{-1})
U liquid spreading velocity (m s^{-1})
V volume at time t (m^3)
V_L actual volume of cryogen spilled (m^3)
V_o effective volume of cryogen spilled, $\rho_L V_L/\rho$; (m^3)
w width of channel (m)
x distance (m)
$x_{e_{nb}}$ actual length of spill tube (m)
x_e characteristic distance (m); $[(V_o/w)^3 g^{\star}/(\dot{M}/\rho)^2]^{1/5}$
$x^{\star}_{nb}$ $x/x_{e_{nb}}$
$x^{\star}$ x/x_e
ϵ conduction parameter used in eqn. (14); ϵ_o, initial parameter in eqn. (14)
λ parameter in eqn. (7)
η parameter in eqn. (9)
ρ effective cryogen density (kg m^{-3}); ρ_w, density of water; ρ_L, true saturated liquid cryogen density; ρ_V, true saturated vapor cryogen density

Subscripts

LE leading edge
max maximum

1. Introduction

Liquefied petroleum gas (LPG) is often transported in bulk within large insulated tankers. An accidental spill of this cryogenic liquid onto water would lead to the formation of a combustible cloud as LPG boils well below ambient water temperature. To evaluate the potential hazards from accidents in marine transport requires reliable data on the boiling and spreading rates of LPG on water.

Most prior spill studies, both experimental and theoretical, have considered only liquefied natural gas (LNG) or liquid methane. In one instance, however, spills of propane and LPG were made on a confined area surface [1]. The apparatus consisted of an adiabatic calorimeter half-filled with water placed on a load cell to monitor continuously the system mass. For a rapid spill of propane or LPG, the initial boiling rate was found to be extremely rapid with immediate ice formation. Within a second or so, the boiling rate dropped and subsequent vaporization was well described by a moving-boundary model [2]. As will be seen later, many of these same characteristics were also observed in unconfined spills of LPG.

2. Experimental method

An experimental apparatus was constructed to measure the rates of boiling and spreading of cryogenic liquids on a water surface. Instantaneous spills were to be simulated, and the flow configuration was one-dimensional.

The cryogenic liquids were prepared by condensing cylinder gases in a vessel cooled by external coils in which liquid nitrogen was evaporating. Heat transfer from the nitrogen coils to the condensing vessel was through *n*-butanol which was used as a bath fluid.

The test apparatus is shown in schematic fashion in Fig. 1. The flow trough was made from a 4 m Plexiglas tube about 16.5 cm inside diameter. The tube was level and half-filled with water. At one end of the tube a distributor was placed. This unit was fabricated from a Lexan polycarbonate tube set in a vertical manner. A spring-loaded piston was installed so that, upon release, it would expose a side port to allow rapid delivery of the cryogen onto the water surface. The maximum liquid capacity of the distributor was about 3 liters, and the side-port area (when fully opened) was 48 cm^2. A transverse section of the distributor is shown in Fig. 2. Pressures in the distributor were held at ambient values with a vent valve.

Water, cryogen, and vapor temperatures were monitored by thermocouples. Eight thermocouples were used in the vapor space and were spaced at about 0.5 m intervals. Twenty-seven thermocouples were introduced through the bottom of the water trough and the junctions positioned on the water surface. Temperature changes as read from these thermocouples were used to determine the rate of spreading of the spilled cryogen.

At the end of the trough where evolved vapor left the tube, any water wave was dampened by a wedge of stainless wool. A high-speed motion pic-

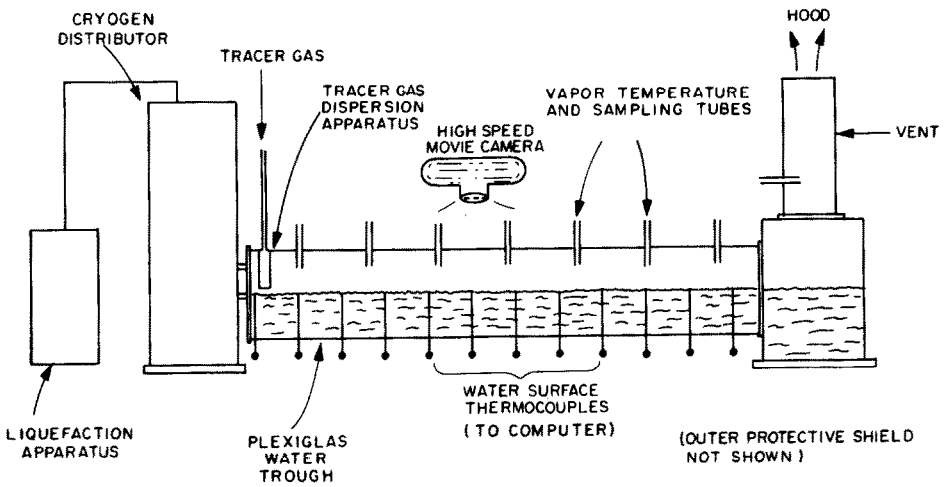

Fig. 1. Schematic of spill/spread/boil apparatus.

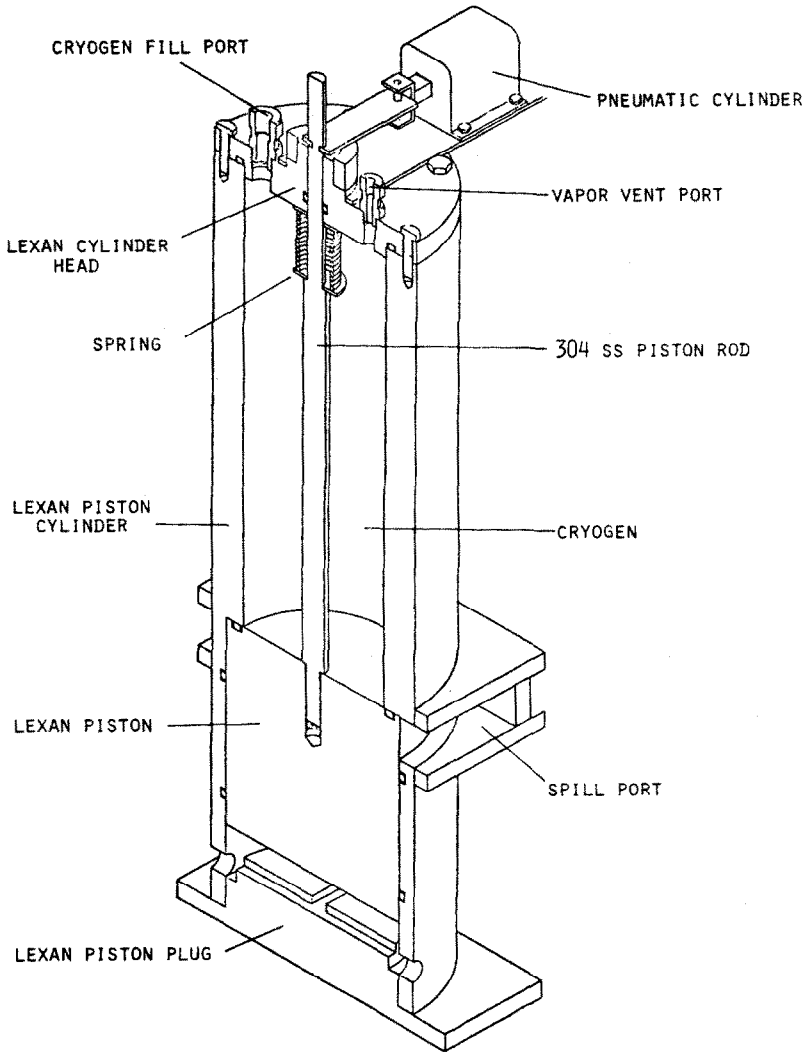

Fig. 2. Transverse view of cryogen distributor.

ture camera could be positioned where desired to obtain pictures of the spreading and boiling processes.

The local boil-off rates of the cryogen were obtained in an indirect manner. A tracer gas, carbon dioxide, was injected continuously at a known rate through a dispersion device located just downstream of the distributor. Eight vapor sampling stations were positioned adjacent to the vapor thermocouples along the tube. Each station had the capacity to collect six separate samples in 25 cm^3 bulbs. A cut-away view of one of the stations is shown in Fig. 3. Before a test, each bulb was purged and pressurized with argon to about 1.4

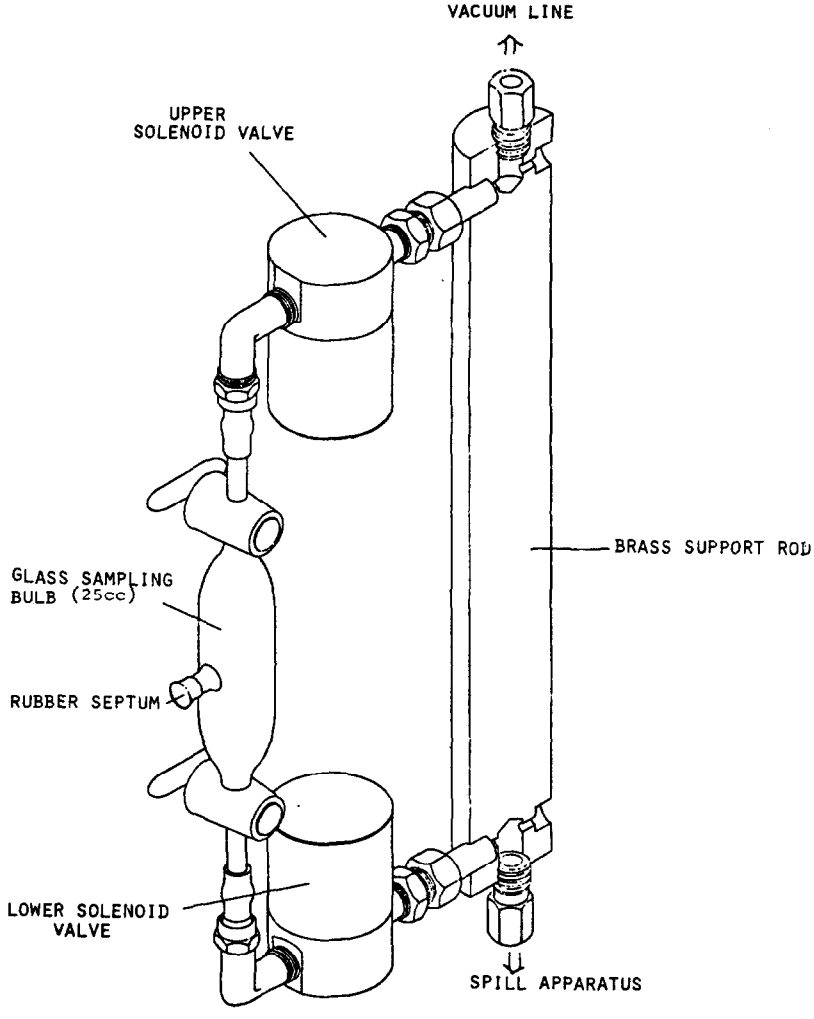

Fig. 3. Isometric cut-away view of vapor sampling station.

bar. During an experiment, a lower solenoid valve would open just prior to sampling; expansion of the argon through the sampling line would purge this section of any previous gas. The upper solenoid valve, which connected the sampling bulb with a vacuum system, was then opened and a vapor sample drawn into the bulb. Sampling ceased with simultaneous closure of both solenoids. A complete sampling required one second.

The actuation of all sampling valves was controlled by a programmed sequencer.

From vapor temperature and gas compositions, in conjunction with knowledge of the tracer carbon dioxide flow rate, it was possible to estimate boiling rates as a function of position and time. This will be described later.

More complete details of the apparatus, analysis procedures, and safety precautions are covered elsewhere [3].

3. Local boiling rates

As noted earlier, the local boiling rates of the cryogen were determined from vapor compositions and temperatures and by employing the constant, known flow rate of the carbon dioxide tracer gas. Referring to Fig. 4, and

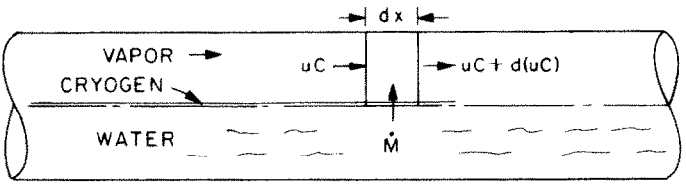

Fig. 4. Mass balance to determine local boiling rates.

assuming the tracer gas and hydrocarbon vapors are well mixed at any given axial location, one may write mass balances for both the tracer and hydrocarbon,

$$\frac{\partial C_T}{\partial t} = -\frac{\partial (uC_T)}{\partial x} \tag{1}$$

$$\frac{\partial C_H}{\partial t} = -\frac{\partial (uC_H)}{\partial x} + \frac{w}{A}\dot{M} \tag{2}$$

The concentrations of the tracer carbon dioxide (C_T) and the hydrocarbon (C_H) were obtained by gas chromatographic analyses of the vapor samples taken during a test. These concentrations were corrected to the true vapor temperature using data taken with the vapor thermocouples. To obtain the boiling rate $\dot{M}$, eqns. (1) and (2) were rewritten in a finite difference form to allow for discrete time and distance intervals. Solution of these equations was then accomplished with experimental C_T, C_H values at various positions and times and by using the initial condition that at $x = 0$, any time, the vapor was pure carbon dioxide flowing at a known, constant velocity.

4. Spreading–boiling model

To describe the spreading and boiling of a cryogenic liquid on a water surface in a one-dimensional configuration, the continuity equation may be written as:

$$\frac{\partial h}{\partial t} + \frac{\partial}{\partial x}(hU) + \frac{\dot{M}}{\rho} = 0 \tag{3}$$

Any acceleration across the cryogen layer thickness (h) is neglected. U is the local spreading velocity and $\dot{M}$ the local vaporization rate; h, U, and $\dot{M}$ are functions of axial position (x) and time (t). ρ is the "effective" cryogen density and is assumed constant. The estimation of ρ is discussed later.

Only the gravity—inertial flow regime is considered. Assuming the cryogen is in hydrostatic equilibrium in the vertical direction, the equation of motion becomes:

$$\frac{\partial U}{\partial t} + U\frac{\partial U}{\partial x} + g^{\star}\frac{\partial h}{\partial x} = 0 \tag{4}$$

where $g^{\star}$ is a corrected gravitational acceleration to account for differences between the density of water (ρ_w) and the effective cryogen liquid density (ρ):

$$g^{\star} = g\,(\rho_w - \rho)/\rho_w \tag{5}$$

The boundary conditions employed are:

$$U = 0, x = 0 \tag{6}$$

and

$$U_{LE} = (\lambda g^{\star} h_{LE})^{1/2} \tag{7}$$

The first implies that, at the spill location, there is a negligible horizontal velocity component. The second condition is one used in nonboiling liquid spreading studies and states that the leading edge velocity is proportional to the square root of the cryogen layer thickness at the leading edge. λ is an experimentally determined parameter and is probably somewhat apparatus-dependent. Values range from 1 to 2. Oil slick studies by Suchon [4] yielded a value of $\lambda = 1.4$. As noted later, pentane spread experiments in the present equipment suggested a value of $\lambda = 1.64$ would be more appropriate for the one-dimensional apparatus used here.

There is no analytical solution for eqns. (3) and (4) and a numerical technique employing the method of characteristics was used in this work. A brief discussion of the procedure is given in the Appendix. More complete details and a computer algorithm are available elsewhere [3]; Muscari [5] describes a similar method to treat radial spills.

The proposed model considers the entire spill process as being initiated at a point. This geometric idealization leads to unmanageable singularities in eqns. (3) and (4) at $x = 0$, $t = 0$. These difficulties can be avoided by initiating the spill model at a very small time, as opposed to $t = 0$, where it is assumed that the spill process up to this time can be described adequately by Hoult's [6] analytical solution for the spreading of a nonvolatile liquid on water. The justification of this treatment is given elsewhere [3].

To verify the numerical technique, calculations were first made for the nonboiling case where $\dot{M} = 0$. In this instance an analytical solution is available [6—8]. With V_L the volume of liquid spilled, for a one-dimensional spread,

$$x/V_L^{1/3} = \eta\ [(g^\star/w)^{1/2}\ t]^{2/3} \tag{8}$$

where η is related to the parameter λ of eqn. (7) by

$$\eta = \left(\frac{4}{9\lambda} - \frac{2}{27}\right)^{-1/3} \tag{9}$$

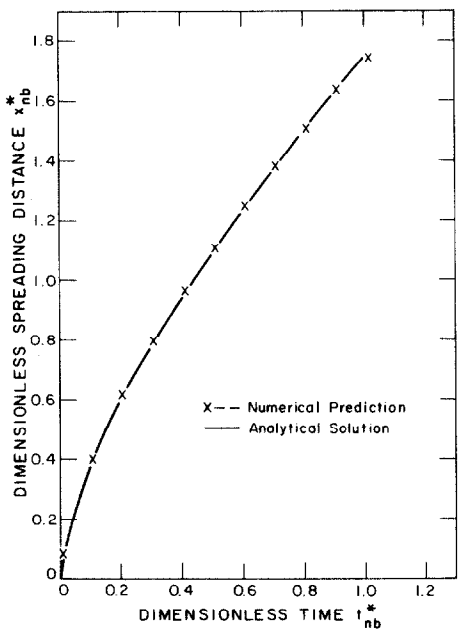

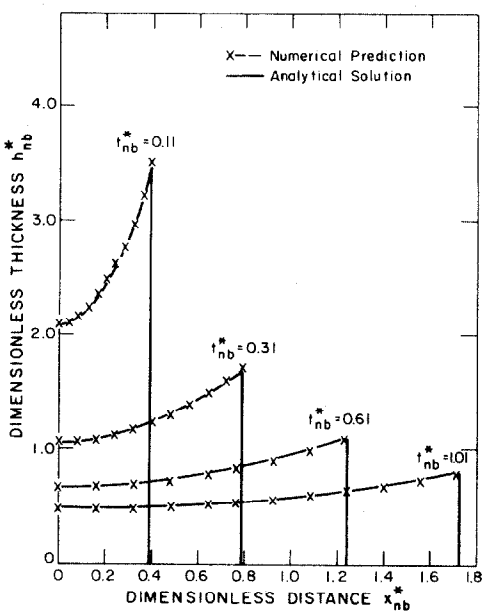

Fig. 5. One-dimensional spreading curves in the gravity—inertia regime for a nonvolatile liquid spilled on water. Numerical prediction compared with Hoult's analytical solution [6].

Fig. 6. Dimensionless thickness profile for a nonvolatile liquid spreading on water in the gravity—inertia regime. Numerical prediction and analytical solution compared.

Using a value of $\lambda = 1.64$, comparisons of the analytical results with those found from the numerical procedure are given in Figs. 5 and 6. Axial distances and times have been nondimensionalized to show the general case. The agreement is excellent. Note that the liquid film is predicted to be thickest at the leading edge.

For the case where $\dot{M}$ is non-zero, but is a constant independent of time and position, the general numerical solutions are shown in Figs. 7 and 8 for

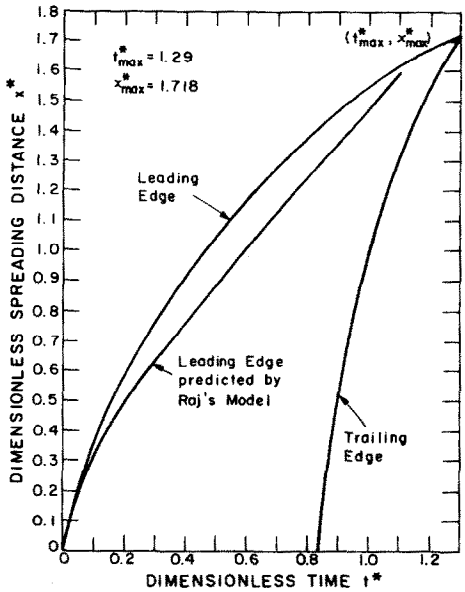

Fig. 7. Paths of the leading and trailing edges predicted by the numerical model for the case of constant heat flux. The corresponding prediction from Raj's model also shown.

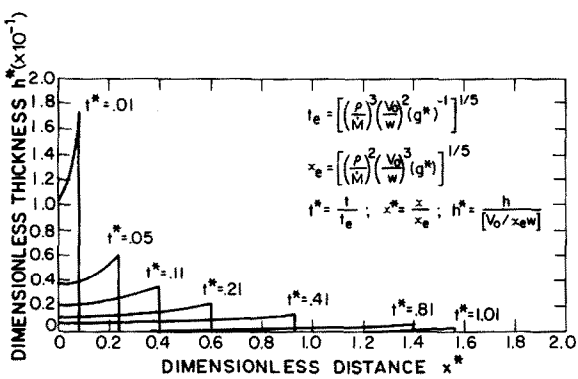

Fig. 8. Dimensionless thickness profile predicted by the numerical model for the case of constant heat flux.

a one-dimensional spill. Film thickness profiles are similar to those found for the nonboiling case, but the spreading distance graph indicates important differences. For the boiling situation, evaporation of the cryogen leads to both a leading and a trailing edge. The intersection of these curves specifies the time and position when all cryogen has evaporated.

Also shown in Fig. 7 is the leading edge trajectory as predicted by the one-dimensional spreading model of Raj [9]. This model is similar to the

radial spreading analysis of Raj and Kalelkar [10]. Instantaneous spills were assumed and the gravitational spreading force was equated to the inertial resisting force,

$$F_{gr} = w\,(h^2/2)\,\rho g^{\star}$$
$$F_{in} = -\,kwxh\rho\;\mathrm{d}^2x/\mathrm{d}t^2 \tag{10}$$

h is a mean thickness of the cryogen layer and k is introduced to account for the fact that the entire mass of cryogen is not being accelerated at the leading edge acceleration $\mathrm{d}^2x/\mathrm{d}t^2$. Vaporization is taken into consideration by

$$V(t) = V_o - (w/\rho) \int_0^t \dot{M}x\mathrm{d}t = wxh \tag{11}$$

with V_o the initial volume of the spill and $\dot{M}$ the boiling rate. $\dot{M}$ is assumed to be a constant and eqns. (10) and (11) solved by a first-order perturbation solution that matches eqns. (8) for the nonboiling case,

$$x^{\star} = 1.39\,t^{\star 2/3} + 0.097\,t^{\star 7/3} \tag{12}$$

where $x^{\star} = x/x_e$ and $t^{\star} = t/t_e$ with x_e and t_e defined in Fig. 8 and in the Notation. No trailing edge is predicted by this model and the maximum distance before complete evaporation is given by $t^{\star}_{max} = 1.09$, $x^{\star}_{max} = 1.59$. These values differ somewhat from the $t^{\star}_{max} = 1.29$, $x^{\star}_{max} = 1.72$ predicted from the numerical spreading–boiling case.

The case of variable $\dot{M}$ is considered later when the experimental data are discussed.

In the modeling described above, it was stated that the *effective* cryogen density was employed. The motivation for introducing this concept lies in the visual observation that the cryogen film is not homogeneous but contains rising vapor bubbles by virtue of the vaporization process occurring at the interface. The vapor generation rate is clearly proportional to the boiling rate $\dot{M}$. Bubble rise velocities were estimated from the buoyancy and drag forces acting on the bubble. In most instances, the bubble rise velocity was found to be in a narrow range of 20 to 30 cm s^{-1} and depended primarily upon the cryogen properties. A simple volume balance then led to the approximate result that

$$\rho = \rho_L \left(1 - \frac{\dot{M}}{\rho_V u_B}\right) \tag{13}$$

where ρ_L and ρ_V are the saturated liquid and vapor densities and u_B is the average bubble rise velocity. u_B was chosen to be about 26 cm s^{-1} for LPG and propane while $u_B \sim 24$ cm s^{-1} was found to be more reasonable for the lighter cryogens such as liquid nitrogen and methane (or LNG).

5. Results and discussion

It was first necessary to measure the spreading rates of nonboiling liquids in order to determine the value of the parameter λ in eqn. (7) that would be applicable for the present test apparatus. For such liquids, eqn. (8) should be applicable.

Liquid *n*-pentane (precooled to 230 K) was used as the test fluid. Eleven spills were made with initial spill volumes varying from 0.5 to 3 liters. The spreading distance is shown as a function of time in Fig. 9, and the slope

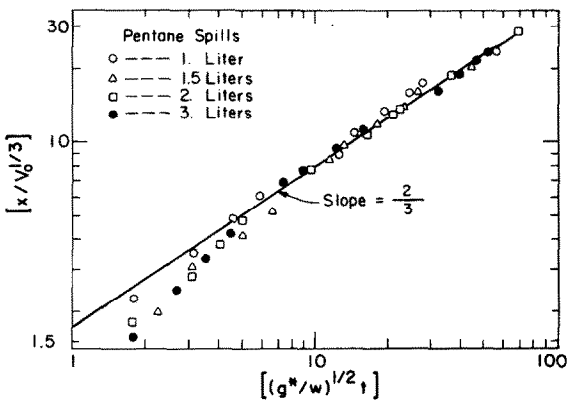

Fig. 9. Dimensionless correlation of spreading distance with time for pentane spills.

agrees with that predicted by eqn. (8). The value of η determined from the straight-line section of the graph is 1.72 and, with eqn. (9), $\lambda = 1.64$. The scatter at short times reflects the uncertainty in defining an absolute value to the starting time.

A few exploratory spills were made with liquid nitrogen and methane; more work on these liquids is in progress and the results will be reported in a later paper.

Most experiments were conducted with liquid propane or with propane containing small concentrations of ethane and/or *n*-butane to simulate liquefied petroleum gas (LPG). Twenty-four tests were run. As with *n*-pentane, initial spill volumes ranged from 0.5 to 3.0 liter.

In a descriptive sense, propane and LPG spills have a different character from liquid nitrogen or methane spills. The latter spread smoothly and ice forms slowly after the cryogenic liquid front has passed. Propane and LPG boil violently with immediate ice formation. For the size of spills studied here, the ice roughness was such as to impede the spreading in some instances. Also, as the ice cooled to liquid propane temperatures, it sometimes cracked and allowed liquid propane to seep between and even under the ice. The subsequent violent boiling would often enlarge the initial crack or even

move the ice so that at the end, the surface resembled rough blocks of ice wedged together. Clearly the relatively simple model described earlier would only provide an approximate resemblance to such a chaotic phenomenon.

Gas analyses did provide a reasonable picture of the heat flux function. Initially as the spreading propane or LPG contacted water, a brief violent boiling period resulted. As soon as ice was formed, however, the boiling rate decreased rapidly and studies of the motion pictures revealed a smooth boiling process. The period of time for the violent boiling to cease was about 1 s. Expressed in an analytical manner,

$$\dot{M}\Delta H_v = \dot{Q} = \begin{cases} \epsilon_o & 0 < t \leqslant 1 \text{ s} \\ \epsilon(t - t_o)^{-1/2} & t > 1 \text{ s} \end{cases} \tag{14}$$

In these relations t is the actual time after contact of the propane (or LPG) with water, and t_o is given by

$$t_o = 1 - (\epsilon/\epsilon_o)^2 \tag{15}$$

to insure that both portions of eqn. (14) yield $\dot{Q} = \epsilon_o$ at $t = 1$ s.

The term ϵ_o specifies the heat flux during the ill-defined, rapid boiling period, $0 < t \leqslant 1$ s. A value of $\dot{Q} \sim 10^3$ kW m^{-2} was chosen. The parameter ϵ is related to the properties of the propane and water ice by a simple moving boundary value model [2]. For propane—water, $\epsilon \sim 154$ kW m^{-2} s$^{-1/2}$.

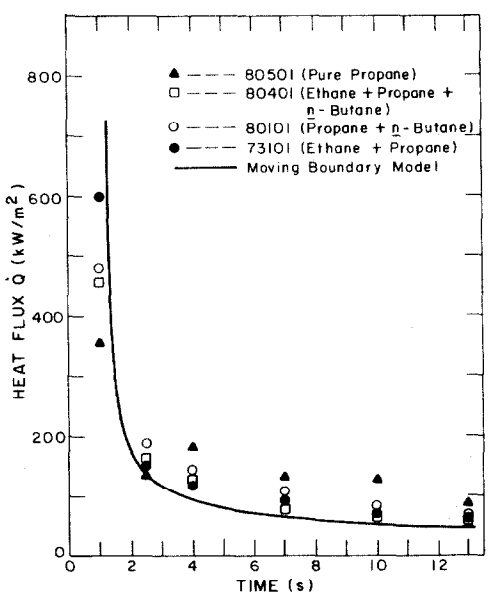

Fig. 10. Local boil-off rate curves for propane and LPG spills at the first sampling station. Experimental data compared with predictions from moving boundary model.

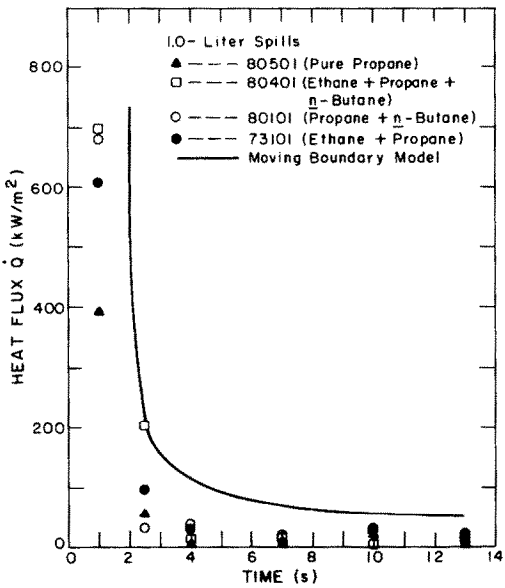

Fig. 11. Local boil-off rate curves for propane and LPG spills at the second sampling station. Experimental data compared with predictions from moving boundary model.

Using this approximate heat transfer model, predicted heat fluxes are compared with those measured experimentally in Figs. 10 and 11. In Fig. 10, the heat flux is the average between the distributor and first sampling station. Agreement between the model and data is quite satisfactory. Note that no prediction is shown for times less than 1 s. In this domain, the model assumes $\dot{Q}$ is constant at 10^3 kW m^{-2}. The dramatic decrease in heat flux results from ice formation with the rate-determining step that of conduction through the growing ice shield. Data and model predictions for the area between the first and second sampling stations are given in Fig. 11. In this instance, the experimental data lie below those predicted. The explanation for the difference is simply that, in most instances, the propane or LPG boiled so rapidly that, even with the larger spills, no liquid ever reached the second station. Thus the *computed* average $\dot{Q}$ exceeded that actually measured.

Assuming that the heat transfer model given above is applicable, the spreading—boiling model was used to estimate the spreading rate of the cryogen. Some typical results are shown in Fig. 12. While at first glance it might appear that the model yielded a satisfactory prediction, a closer examination shows that the ice roughness has slowed the spreading, and definite *pauses* can be seen as the ice jams temporarily halted the spreading process. One would expect, however, that the model would be more accurate for larger spills when the cryogen thickness would significantly exceed the ice roughness.

In Table 1, the average experimental and computed spreading distances

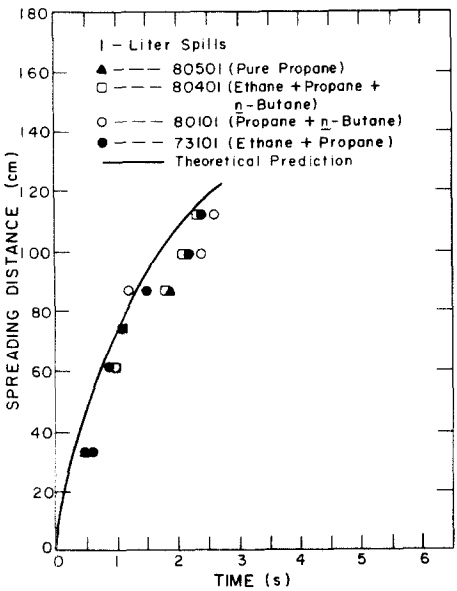

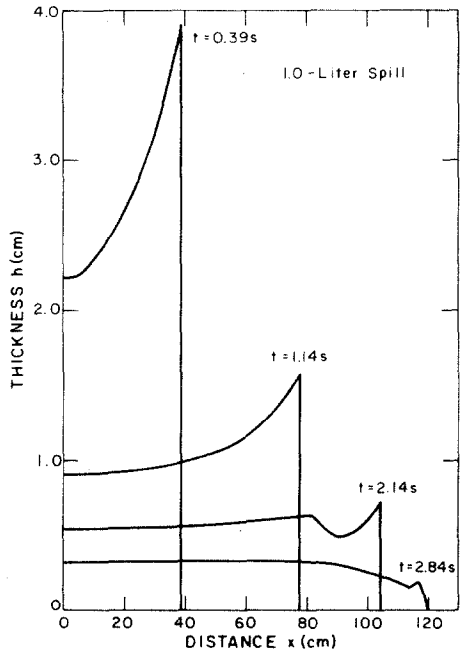

Fig. 12. Spreading curves for propane and LPG spills. Experimental data and numerical predictions compared.

Fig. 13. Thickness profile predicted by the numerical model for liquid propane spreading on water.

TABLE 1

Maximum spreading distance for propane and LPG spills

Volume spilled (liter)	Maximum spreading distance (cm)	
	Experiment	Theory
0.5	68	79
0.75	90	101
1.0	110	120
1.5	150	153
2.0	163	182

are shown for various sized propane and LPG spills. (No differences were noted in either heat fluxes or spreading rates between pure propane and LPG spills.)

The analytical model also leads to predictions regarding the thickness profile for the propane/LPG tests. The results for a 1 liter spill are shown in Fig. 13. These may be compared with those in Fig. 8 where a constant boiling rate was assumed. The rapid attenuation in heat flux for the propane/LPG case inhibits the formation of a trailing edge and leads, at longer times, to a profile where the thickest film is at the spill point.

6. Concluding remarks

An experimental apparatus was built to measure simultaneously the boiling and spreading rates of cryogenic liquids spilled on water. Most experiments were conducted with liquid propane and LPG; later work will cover liquefied natural gas. An analytical model was developed to describe the spreading rate when boiling rates were known as a function of time after coverage by the liquid. To describe the boiling of propane on water, a rapid, but brief, constant rate period was postulated to be followed by a decreasing boiling rate as ice grew in thickness under the boiling propane. This heat transfer model is similar to that developed earlier to describe the boiling of propane in a confined area calorimeter. The experimental measurements of propane vaporization agreed well with the model. Also, the spreading rates were reasonably well predicted by the spreading model except that the rough ice surface did impede the spreading rate somewhat for the small spills used in this study.

All experimental and theoretical studies were for a one-dimensional case. There is no reason to expect that a boiling–spreading model for radial spills, based on the same basic ideas, would not be applicable.

One interesting aspect of the model is that it predicts that, if the boiling rate does not decrease rapidly with time — or is constant — then there will be both a leading and trailing edge to the spilled liquid. This finding will affect the boiling area at any given time and, therefore, the total vapor evolution rate. For propane spills, this phenomenon does not occur and the maximum liquid thickness is at the spill position.

Acknowledgement

This work was supported by a grant from the Department of Energy and their assistance is gratefully acknowledged. In addition, the Gas Research Institute provided partial funding for the experimental equipment. Professor James A. Fay was very helpful in developing the analytical model.

Appendix

An outline of the spreading–boiling model using the method of characteristics — the one-dimensional case

See [11, 12] for more complete descriptions. Since the cryogen height h and its velocity U are functions of axial position x and time t, an expansion of these variables yields:

$$dh = \frac{\partial h}{\partial x} dx + \frac{\partial h}{\partial t} dT \tag{A.1}$$

$$dU = \frac{\partial U}{\partial x} dx + \frac{\partial U}{\partial t} dt \tag{A.2}$$

Eqns. (3), (4), (A.1), and (A.2) can then be rearranged to:

$$U\frac{\partial h}{\partial x}+\frac{\partial h}{\partial t}+h\frac{\partial U}{\partial x}=-\frac{\dot{M}}{\rho}$$

$$g^{\star}\frac{\partial h}{\partial x}+U\frac{\partial U}{\partial x}+\frac{\partial U}{\partial t}=0 \tag{A.3}$$

$$\mathrm{d}x\frac{\partial h}{\partial x}+\mathrm{d}t\frac{\partial h}{\partial t}=\mathrm{d}h$$

$$\mathrm{d}x\frac{\partial U}{\partial x}+\mathrm{d}t\frac{\partial U}{\partial t}=\mathrm{d}U$$

Eqn. (A.3) may be viewed as a set of simultaneous linear equations in the unknowns $\partial h/\partial x$, $\partial h/\partial t$, $\partial U/\partial x$, and $\partial U/\partial t$. As the characteristic directions depend only on the coefficients, any of the unknowns may be used to find these characteristic directions. For instance, solving for $\partial h/\partial x$,

$$\frac{\partial h}{\partial x}=\begin{vmatrix} -\dot{M}/\rho & 1 & h & 0\\ 0 & 0 & U & 1\\ \mathrm{d}h & \mathrm{d}t & 0 & 0\\ \mathrm{d}U & 0 & \mathrm{d}x & \mathrm{d}t \end{vmatrix} \Big/ \begin{vmatrix} U & 1 & h & 0\\ g^{\star} & 0 & U & 1\\ \mathrm{d}x & \mathrm{d}t & 0 & 0\\ 0 & 0 & \mathrm{d}x & \mathrm{d}t \end{vmatrix} \tag{A.4}$$

To establish the characteristic curves on the x—t and U—h plane across which $\partial h/\partial x$, $\partial h/\partial t$, $\partial U/\partial x$, and $\partial U/\partial t$ are indeterminate, the determinants of eqn. (A.4) are set equal to zero. The numerator and denominator yield, respectively,

$$\frac{\mathrm{d}U}{\mathrm{d}h}=\left(U-\frac{\mathrm{d}x}{\mathrm{d}t}\right)\frac{1}{h}-\dot{M}/\rho\quad\left(1-U\frac{\mathrm{d}t}{\mathrm{d}x}\right)\frac{1}{h}\frac{\mathrm{d}x}{\mathrm{d}h} \tag{A.5}$$

$$(U^2-g^{\star}h)\left(\frac{\mathrm{d}t}{\mathrm{d}x}\right)^2-2U\left(\frac{\mathrm{d}t}{\mathrm{d}x}\right)+1=0 \tag{A.6}$$

Eqn. (A.6) is hyperbolic and yields two real solutions for $\mathrm{d}t/\mathrm{d}x$:

$$\left(\frac{\mathrm{d}t}{\mathrm{d}x}\right)=[U+(g^{\star}h)^{1/2}]^{-1};\quad\left(\frac{\mathrm{d}t}{\mathrm{d}x}\right)=[U-(g^{\star}h)^{1/2}]^{-1} \tag{A.7}$$

Substitution of eqn. (A.7) into (A.5) will produce characteristic curves on the U—h plane.

A numerical procedure can then be developed beginning with known values of U and h at any x, with $t=0$. U and h may then be found as a function of x for later times. $\dot{M}$ may be set equal to zero (to simulate a nonboiling case) or it may be specified as a constant or as a function of x and t if the functionality has been determined from experimental or theoretical considerations.

References

1 R.C. Reid and K.A. Smith, Behavior of LPG on water, Hydro. Proc., April 1978, p. 117.
2 E.R.G. Eckert and R.M. Drake, Analysis of Heat and Mass Transfer, McGraw-Hill, New York, 1972.
3 H.-R. Chang, Simultaneous boiling and spreading of liquefied petroleum gas on water, Sc.D. Thesis, M. I. T., Cambridge, MA, 1981.
4 W. Suchon, An experimental investigation of oil spreading over water, M.S. Thesis, M. I. T., Cambridge, MA, 1970.
5 C.C. Muscari, The evolution of liquid natural gas on water, M.S. Thesis, MIT, Cambridge, MA, 1974.
6 D.P. Hoult, Oil spreading on the sea, Annu. Rev. Fluid Mech., 4 (1972) 341.
7 T.K. Fannelop and G.D. Waldman, Dynamics of oil slicks, AIAA J. 10 (4) (1972) 506.
8 J.A. Fay, Physical processes in the spread of oil on a water surface, Conf. Prev. Control of Oil Slicks, Am. Pet. Inst., Washington, DC, 1971.
9 P. Raj, Personal communication, 1979.
10 P. Raj and A. Kalelkar, Assessment Models in Support of the Hazard Assessment Handbook (CG-446-3), U.S. Coast Guard, NTIS AD776617, 1974.
11 A.H. Shapiro, The Dynamics and Thermodynamics of Compressible Fluid Flow, Vol. 1, Ronald Press, New York, 1953.
12 P.A. Thompson, Compressible Fluid Dynamics, McGraw-Hill, New York, 1972.